Geophysical Research Letters

RESEARCH LETTER
10.1029/2018GL081799

Topographic Controls on the Extension and Retraction of Flowing Streams

Jeff P. Prancevic[1] and **James W. Kirchner**[1,2]

[1]Department of Environmental Systems Science, ETH Zürich, Zürich, Switzerland, [2]Snow and Landscape Research WSL, Swiss Federal Institute for Forest, Birmensdorf, Switzerland

Key Points:
- Some flowing stream networks lengthen dramatically as their catchments become wetter, whereas others change much less
- This tendency for networks to extend and retract can be predicted from down-valley changes in slope, drainage area, and curvature
- As valleys become more sharply incised downstream, subsurface transmissivity decreases, which helps stabilize flowing stream length

Supporting Information:
- Supporting Information S1

Correspondence to:
J. P. Prancevic,
jeff.prancevic@gmail.com

Citation:
Prancevic, J. P., & Kirchner, J. W. (2019). Topographic controls on the extension and retraction of flowing streams. *Geophysical Research Letters*, *46*, 2084–2092. https://doi.org/10.1029/2018GL081799

Received 3 JAN 2019
Accepted 29 JAN 2019
Accepted article online 1 FEB 2019
Published online 15 FEB 2019

Abstract Flowing stream networks extend and retract as their surrounding landscapes wet up and dry out, both seasonally and during rainstorms, with implications for aquatic ecosystems and greenhouse gas exchange. Some networks are much more dynamic than others, however, and the reasons for this difference are unknown. Here we show that the tendency of stream networks to extend and retract can be predicted from down-valley changes in topographic attributes (slope, curvature, and contributing drainage area), without measuring subsurface hydrologic properties. Topography determines where water accumulates within valley networks, and we propose that it also modulates flow partitioning between the surface and subsurface. Measurements from 17 mountain stream networks support this hypothesis, showing that undissected valley heads have greater subsurface transport capacities than sharply incised valleys downstream. In catchments where broad valley heads rapidly transition to sharply incised valleys, subsurface transport capacity decreases abruptly, stabilizing stream length through wet and dry periods.

Plain Language Summary Although stream networks are represented as fixed blue lines on maps, the actual extent of flowing water dynamically adjusts as landscapes become wetter and drier. This is an old observation, but one without a satisfying physical explanation. Intuitively, flowing streams extend during wetter periods, as smaller parts of the landscape are able to supply enough water to support streamflow. But the supply of water is only part of the story, because some parts of the landscape may have greater capacity to move supplied water through the subsurface without streamflow, affecting where water ultimately emerges. In this study, we use observations from 17 mountainous landscapes to show that topography can be used to predict both the supply of water and the capacity to move that water through the subsurface. Consequently, topographic maps can tell us how much a stream network will extend as its surrounding landscape becomes wetter. This helps us predict how dynamic (or, conversely, stable) stream networks will be during rainstorms, droughts, and longer-term climatic shifts.

1. Introduction

In most landscapes, water moves downhill primarily by seeping through the shallow subsurface and by flowing through stream channels. The partitioning of water above and below the surface is important for a wide range of Earth-surface processes: the extent and connectivity of surface flows determine the mobility and dispersion of freshwater macroinvertebrates (Clarke et al., 2008); fast-moving surface water is required to move sediment and carve valleys into the landscape (Howard et al., 1994); and the total land area covered by surface water is a key control on carbon-dioxide efflux from continents, as well as dissolved organic carbon (DOC) export in rivers (Allen & Pavelsky, 2018; Aufdenkampe et al., 2011; Zimmer & McGlynn, 2018). The density of stream channels varies across tectonic and climatic settings, and the physical mechanisms driving this regional variability have received considerable attention (e.g., Clubb et al., 2016, Moglen et al., 1998, Tucker & Bras, 1998). However, even within an individual catchment, the density of actively flowing streams can vary by up to an order of magnitude seasonally or during rainstorms (Allen et al., 2018; Blyth & Rodda, 1973; Day, 1978; Godsey & Kirchner, 2014; Goulsbra et al., 2014; Gregory & Walling, 1968; Jensen et al., 2017; Lovill et al., 2018; Roberts & Archibold, 1978; Roberts & Klingeman, 1972; Shaw, 2016; Whiting & Godsey, 2016; Wigington et al., 2005; Zimmer & McGlynn, 2017; Figure 1), and it is unclear what controls the temporal variability in wetted stream length.

In catchments where flowing streams have been mapped multiple-times, wetted stream length (L) increases as a power function of the water discharge at the outlet of the catchment (Q_o),

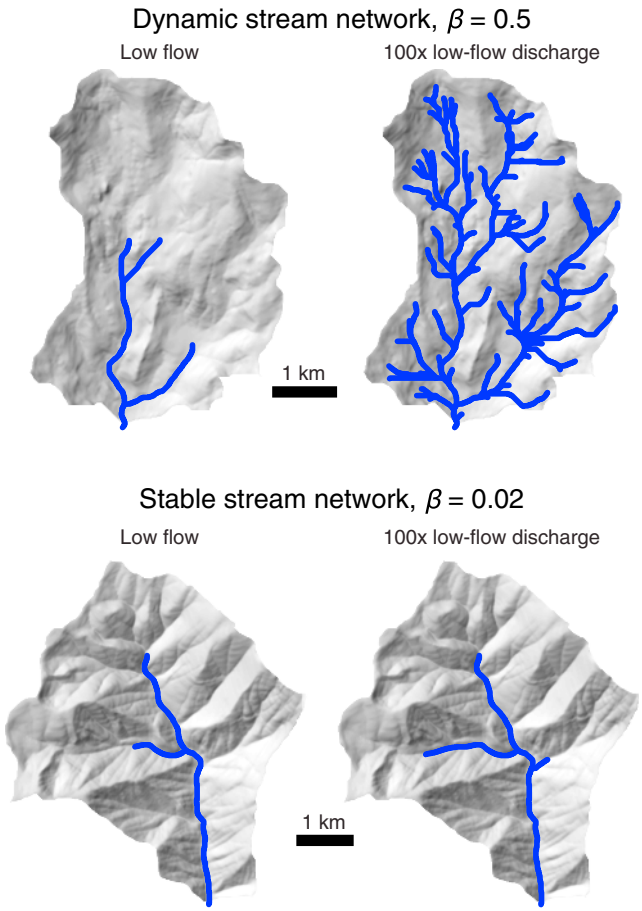

Figure 1. Maps illustrating measured values of β (equation (1)). The left panels show synthetic flowing stream networks during an assumed low-flow discharge. The right panels show the wetted stream networks that would occur under a 100-fold increase in discharge. In the hypothetical highly dynamic network ($\beta = 0.5$), increasing discharge by a factor of 100 causes a 900% increase in stream length. The same increase in discharge causes only a 10% increase in stream length for the less dynamic network ($\beta = 0.02$).

$$L \propto Q_o^{\beta}, \tag{1}$$

with the network extension scaling exponent β varying considerably among catchments (Godsey & Kirchner, 2014; Jensen et al., 2017; $0.02 \leq \beta \leq 0.7$). This wide range in β indicates that some stream networks extend dramatically as catchments become wetter, while others remain nearly fixed in place (Figure 1). The tendency for some networks to be much more dynamic than others must reflect differences in the landscape properties that bring water to the surface. For example, subsurface transport capacity can be sensitive to valley slope (Jensen et al., 2018; Whiting & Godsey, 2016; Wondzell, 2011), sediment size (Costigan et al., 2016; Wondzell, 2011), tectonic structures (Kennedy et al., 1984; Whiting & Godsey, 2016), and river behavior (e.g., incision versus aggradation; Costigan et al., 2016), but attempts to quantitatively relate these properties to stream network dynamics are rare. Two recent studies have attempted to model spatial and temporal patterns of stream connectivity and intermittency in a few well-studied catchments (Jensen et al., 2018; Ward et al., 2018), but these models cannot easily be transferred to other catchments. Consequently, we lack a portable tool for predicting how flowing stream networks will respond to large storms or droughts.

Here we develop a simple theoretical framework that can be used to predict changes in stream network length (which are otherwise difficult to measure) from river discharge and topographic metrics (which are comparatively easy to measure). We calibrate this predictive model using measured values of β from 17 mountainous stream networks in humid and semiarid climates (Godsey & Kirchner, 2014; Jensen et al., 2017; Lovill et al., 2018; Roberts & Klingeman, 1972; Shaw, 1968; Whiting & Godsey, 2016).

2. Mechanistic Framework for Predicting Stream Extension

Flowing streams exist wherever the supplied discharge from upstream (Q) exceeds the transport capacity ($Q_{sub,c}$) of permeable sediment and bedrock underneath the stream channel (Dunne & Black, 1970; Godsey & Kirchner, 2014). If we assume that the supplied discharge is proportional to the local contributing drainage area (A), the instantaneous discharge for each point in the catchment can be expressed as function of the discharge and drainage area at the outlet (Q_o and A_o):

$$Q = Q_o \frac{A}{A_o} \tag{2}$$

The subsurface transport capacity depends on the extent and permeability of the sediment and fractured bedrock in the subsurface, as well as the local hydraulic gradient driving flow (Godsey & Kirchner, 2014; Wondzell, 2011):

$$Q_{sub,c} = aKS \tag{3}$$

where a is the cross-sectional area of the permeable zone, K is the average hydraulic conductivity across a, and S is the local topographic gradient that sets the maximum hydraulic gradient when the subsurface is saturated. We expect that a, K, and S vary spatially, and perhaps systematically as a function of drainage area, but that they do not change significantly over seasonal time scales. Because streamflow reflects the local balance between the supplied discharge (equation (2)) and the subsurface transport capacity (equation (3)), the extension and retraction of flowing streams depends on how A, a, K, and S vary spatially throughout valley networks.

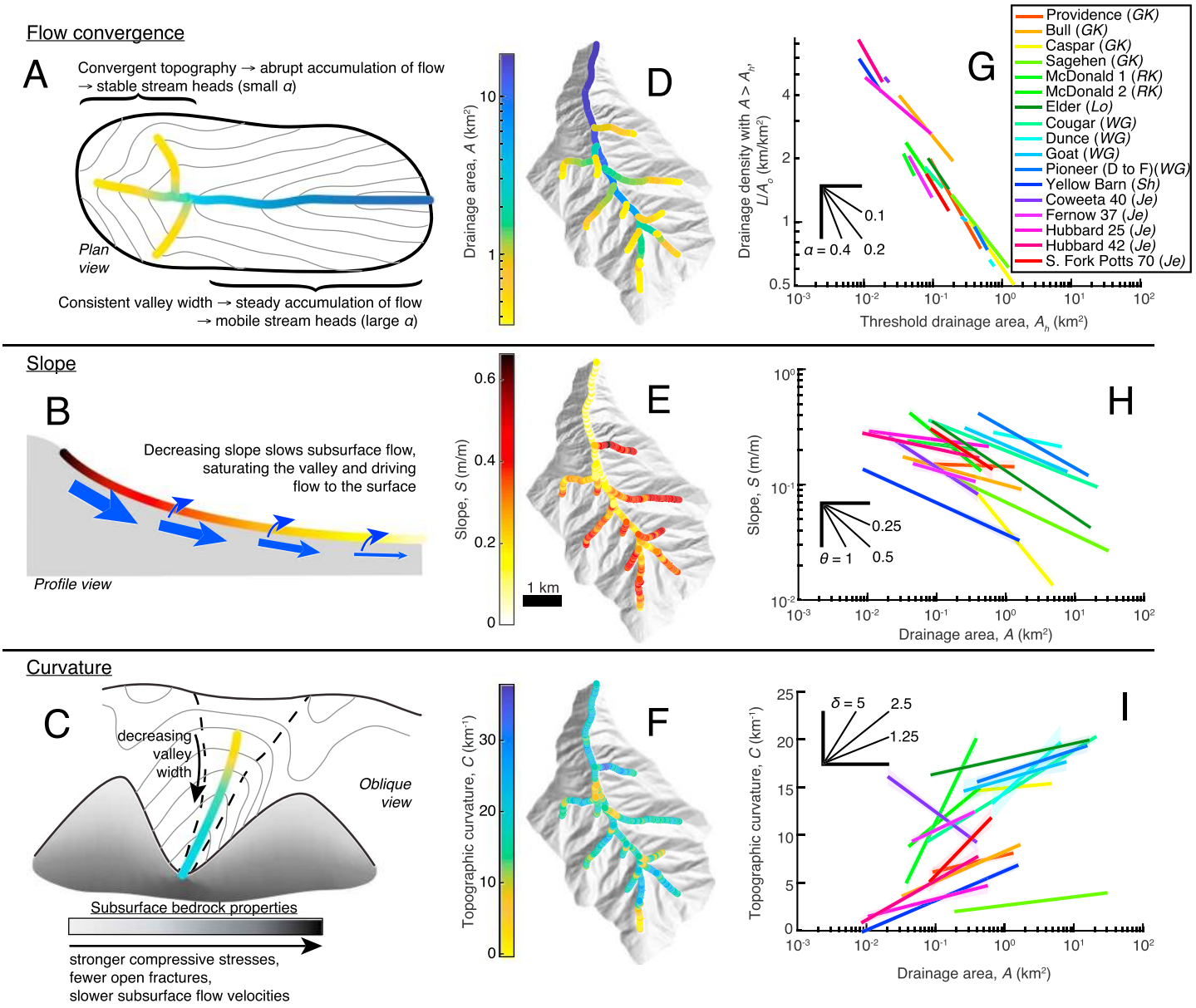

Figure 2. Spatial patterns of topographic attributes and diagrams illustrating their impact on streamflow emergence. (a)–(c) depict how flow convergence, slope, and valley curvature are expected to affect the emergence of streamflow. The valley centerline in each diagram is colored according to the local drainage area, slope, and curvature, and the color scale matches the measured properties shown in maps of Pioneer Creek, ID, in (d)–(f). Similar maps are available for the remaining study sites in Figures S1–S17. (g) displays the robust-fit scaling relationships between drainage density (L/A_o) and threshold drainage area (A_h). (h) and (i) show how valley slope and topographic (Laplacian) curvature scale with drainage area at each site (using robust fitting). The colored lines in all three panels are best fit log–log regression lines (or log linear regressions for (i)). The slopes of these lines are the scaling exponents α and θ, and the curvature coefficient δ. The shaded areas around each line represent the 95% confidence bounds but are often narrower than the lines themselves. Plots displaying the raw data for each study site are provided in Figures S1–S17. The two-letter code following each catchment name in the legend indicates the study that reported the β value for that catchment (Table 1).

We propose that the dynamic extension and retraction of stream networks is shaped by three scaling relationships that relate L to A, a, K, and S. The first scaling relationship expresses how drainage area (and thus discharge) increases nonlinearly with downstream distance due to the convergence of flow paths within catchments (Figure 2d). The spatial pattern of this flow accumulation will influence network behavior (Whiting & Godsey, 2016; Figure 2a), with the stream network's total length L growing and shrinking as a power function of the minimum area A_h where streamflow first appears (Moglen et al., 1998; $L \propto A_h^{-\alpha}$, where α quantifies the convergence of a catchment and is approximately $\alpha \approx 0.5$ for most landscapes;

Figure 2g). The topographic slope of stream channels also tends to decrease as a power function of drainage area ($S \propto A^{-\theta}$; Figures 2b, 2e, and 2h), with scaling exponents that commonly range from $\theta = 0.4$ to 0.6 in mountainous landscapes (Kirby & Whipple, 2012). The third scaling relationship expresses how valley transmissivity (the product of subsurface cross-sectional area and conductivity, $T = aK$) varies with drainage area. Although measurements of the width, thickness, and conductivity of the permeable zone underlying ephemeral channels are generally not available, there are several reasons to expect that T may decrease downstream (discussed below), and thus, we posit a hypothetical scaling relationship with drainage area, $T \propto A^{-\gamma}$.

These three scaling relationships can be combined with equations (2) and (3) to estimate the network extension exponent β in equation (1):

$$L \propto {Q_o}^{\frac{\alpha}{\gamma+\theta+1}} = {Q_o}^{\beta} \qquad \leftrightarrow \qquad \beta = \frac{\alpha}{\gamma+\theta+1} \tag{4}$$

Equation (4) suggests that flowing stream networks will be less dynamic where slope and valley transmissivity decrease rapidly downstream (large γ and θ), which drives water to the surface by reducing the subsurface transport capacity $Q_{sub,c}$ (Figures 2a and 2b). Similarly, where flow paths are highly convergent (small α), rapid downstream accumulation of Q will result in more stable stream heads. If the three scaling exponents for valley slope, transmissivity, and flow convergence are known, then equation (4) predicts how stream networks will extend and retract as landscapes become wetter or drier. The scaling behavior of valley slope and flow convergence can be measured directly from digital elevation models (DEMs; Figures 2d and 2e). Valley transmissivity, however, cannot be easily measured with any existing techniques, and there are no previously published estimates for how transmissivity might vary as a function of drainage area. To address this gap in our ability to predict stream network dynamics, we use equation (4) to calculate γ for 17 mountainous catchments with known values of β: $\gamma = \frac{\alpha}{\beta} - \theta - 1$. We then show that values of γ are related to down-valley gradients in topographic curvature, and we apply the inferred relationship between curvature and transmissivity to predict β values from topographic properties, alone (curvature, slope, drainage area).

3. Downstream Trends of Valley Transmissivity

Our analysis of γ values includes, to our knowledge, the entire global data set of catchments larger than $A_o = 0.35$ km^2, where flowing stream networks have been mapped over a broad range of measured discharges, providing reliable estimates of β (Text S1). We used DEMs from the USGS National Elevation Dataset with 10- or 3-m pixels to measure the topographic scaling exponents, α and θ (Table 1; Text S1). All three measured scaling exponents (β, α, and θ) vary widely among the 17 study sites (Figures 2g, 2h, and 3b; Table 1), reflecting differences in both stream network behavior and topographic configurations. The resulting transmissivity scaling exponents also have a broad range, from $\gamma = -0.6$ to 11 (Figure 3a; Table 1), indicating different spatial gradients in transmissivity among sites. Values of γ that are close to zero indicate that valley transmissivity is fairly constant along the length of headwater valleys. But γ is large at most of our study sites, indicating that transmissivity decreases downstream, sometimes sharply. The most extreme case ($\gamma = 11$ in McDonald Catchment 1) suggests that as the drainage area doubles, the valley transmissivity is reduced by a factor of 2,000. This enormous reduction in transmissivity is required to explain the observed stability of stream network length across a wide range of catchment discharges at this site (Roberts & Klingeman, 1972). Note, however, that our source data, and thus the spatial gradients in transmissivity that we infer from them, are limited to headwater networks, and we do not suggest that transmissivity necessarily continues to decrease downstream through larger river valleys.

Transmissivity is primarily controlled by the composition and configuration of sediment and bedrock below the surface. These subsurface properties are difficult to measure directly, but topography might provide several clues about their spatial patterns. The burial of valley bottoms with sediment, for example, will tend to tend to reduce cross-valley curvature and locally increase transmissivity. Cross-valley curvature also determines the width of the valley bottom where subsurface flow can be distributed. Near drainage divides, valley heads tend to be relatively smooth and un-incised, but farther downstream localized stream incision can narrow valley widths and confine flow laterally (Figure 2c). Curvature also affects the size and distribution of bedrock fractures beneath valley bottoms. Compressive stresses tend to be highest beneath valleys and

Geophysical Research Letters

10.1029/2018GL081799

Table 1
Catchment Statistics and Measurements

Catchment	Location	Study[a]	DEM Resolution (m)	Observed Drainage Densities, L/A_o (km/km^2)		Catchment Area, A_o (km^2)	Mapped Extension Scaling Exponent, β ($L \propto Q_o^{\beta}$)	Drainage Density Scaling Exponent, α ($L \propto A_h^{-\alpha}$)	Slope Scaling Exponent, θ ($S \propto A^{-\theta}$)	Transmissivity Scaling Exponent, γ ($T \propto A^{-\gamma}$)	Curvature Coefficient, δ ($C = \delta \ln A + C_0$)
				Min	Max						
Providence Ck	Sierra Nevada, CA	*GK*	10	0.61	1.95	4.27	0.401 ± 0.061	0.576 ± 0.007	0.020 ± 0.027	0.42 ± 0.22	0.74 ± 0.15
Bull Ck	Sierra Nevada, CA	*GK*	10	1.88	3.91	3.07	0.182 ± 0.022	0.399 ± 0.007	0.165 ± 0.011	1.03 ± 0.27	1.37 ± 0.07
Caspar Ck	California Coast Ranges	*GK*	10	0.50	0.99	8.94	0.310 ± 0.050	0.469 ± 0.008	0.726 ± 0.029	-0.21 ± 0.25	0.30 ± 0.19
Sagehen Ck	Sierra Nevada, CA	*GK*	10	0.57	1.29	30.76	0.312 ± 0.093	0.419 ± 0.005	0.284 ± 0.007	0.06 ± 0.40	0.39 ± 0.02
McDonald 1	Oregon Coast Range	*RK*	3	1.62	2.22	0.44	0.058 ± 0.015	0.484 ± 0.025	0.487 ± 0.019	2.95 ± 1.64	2.59 ± 0.22
McDonald 2	Oregon Coast Range	*RK*	3	1.13	2.37	0.39	0.109 ± 0.040	0.675 ± 0.073	0.081 ± 0.036	10.56 ± 3.26	6.49 ± 0.30
Elder Ck	California Coast Ranges	*Lo*	10	1.43	2.01	16.83	0.175 ± 0.037	0.487 ± 0.004	0.402 ± 0.005	1.38 ± 0.59	0.83 ± 0.07
Cougar Ck	Rocky Mountains, ID	*WG*	10	1.47	1.83	21.22	0.083 ± 0.100	0.379 ± 0.009	0.238 ± 0.005	3.33 ± 5.50	1.96 ± 0.06
Dunce Ck	Rocky Mountains, ID	*WG*	10	0.62	0.68	6.48	0.093 ± 0.013	0.442 ± 0.153	0.126 ± 0.015	3.63 ± 1.78	2.81 ± 0.57
Goat Ck	Rocky Mountains, ID	*WG*	10	1.01	1.06	7.83	0.055 ± 0.024	0.245 ± 0.015	0.257 ± 0.014	3.19 ± 1.96	0.90 ± 0.22
Pioneer Ck	Rocky Mountains, ID	*WG*	10	0.76	0.97	15.74	0.197 ± 0.037	0.595 ± 0.037	0.339 ± 0.006	1.68 ± 0.60	1.03 ± 0.12
Yellow Barn	Appalachian Plateau, NY	*Sh*	10	3.93	5.87	1.58	0.114 ± 0.040	0.490 ± 0.014	0.273 ± 0.010	3.02 ± 1.51	1.35 ± 0.04
Coweeta 40	Blue Ridge, NC	*Je*	3	4.58	4.82	0.40	0.040 ± 0.008	0.384 ± 0.031	0.390 ± 0.030	8.21 ± 2.07	-2.32 ± 0.23
Fernow 37	Appalachian Plateau, WV	*Je*	3	1.34	2.15	0.37	0.180 ± 0.017	0.593 ± 0.026	0.173 ± 0.031	2.12 ± 0.34	1.49 ± 0.17
Hubbard 25	White Mountains, NH	*Je*	10	2.33	6.33	0.57	0.590 ± 0.033	0.280 ± 0.004	0.076 ± 0.012	-0.60 ± 0.03	0.81 ± 0.12
Hubbard 42	White Mountains, NH	*Je*	10	4.64	7.26	0.41	0.240 ± 0.023	0.578 ± 0.012	0.128 ± 0.012	1.28 ± 0.24	1.79 ± 0.13
S. Fork Potts 70	Ridge and Valley, VA	*Je*	10	1.07	1.59	0.64	0.140 ± 0.006	0.542 ± 0.037	0.393 ± 0.034	2.48 ± 0.31	3.26 ± 0.38

Note. General catchment statistics and calculated topographic scaling exponents and coefficients for each catchment used in this analysis. Errors following each of the scaling exponents and coefficients are standard errors.
[a]*GK*: Godsey & Kirchner (2014), *RK*: Roberts & Klingeman (1972), *Lo*: Lovill et al. (2018), *WG*: Whiting & Godsey (2016), *Sh*: Shaw (2016), *Je*: Jensen et al. (2017).

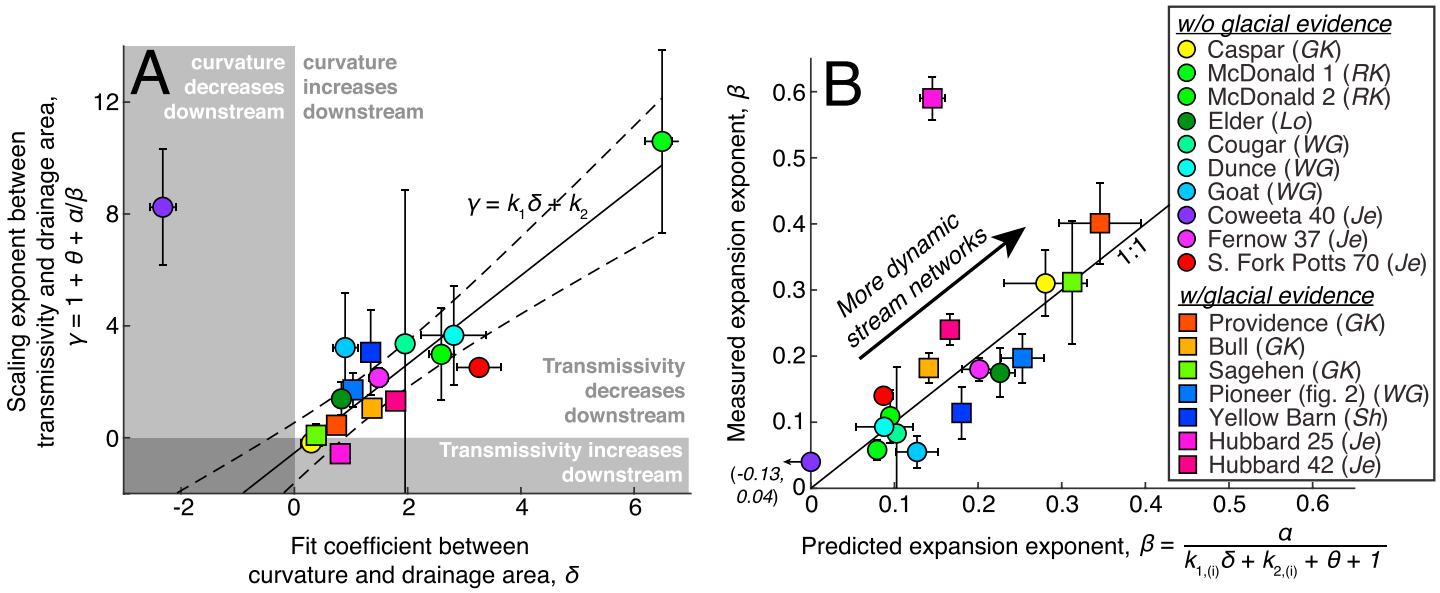

Figure 3. Plots showing how topographic scaling relationships are related to transmissivity and stream network dynamics. (a) shows that the inferred downstream scaling of transmissivity (γ) is roughly proportional to the downstream scaling of valley curvature (δ). The transmissivity scaling exponent γ was calculated using published values of β from mapping studies (Godsey & Kirchner, 2014; Jensen et al., 2017; Lovill et al., 2018; Roberts & Klingeman, 1972; Shaw, 1968; Whiting & Godsey, 2016) and values of θ and α measured from DEMs (Figures 2g and 2h). Values of the drainage area coefficient δ were measured directly from DEMs (Figure 2i). The solid line is the robust-fit regression line ($k_1 = 1.6$ km and $k_2 = -0.51$), and the dashed lines are its 95% confidence bounds. Error bars are 1 standard error. (b) compares values of β that were measured by field mapping against those predicted using only topographic data and jackknifed regression coefficients ($k_{1,(i)}$ and $k_{2,(i)}$) calculated separately for each site by excluding it from regression fits like (a), thus avoiding any redundancy between the predicted and measured values of β. Comparison with the 1:1 line shows that stream network behavior is well predicted by equation (5) for most sites, suggesting that topography can explain much of the variability in β among sites. The two-letter code following each catchment name in the legend indicates the study that reported the β value for that catchment (Table 1).

increase nonlinearly with valley curvature (Flinchum et al., 2018; Miller & Dunne, 1996; Moon et al., 2017). Because compressive stress controls the aperture of bedrock fractures (Min et al., 2004; Rutqvist, 2014), fractures that underlie incised valleys should be less hydraulically conductive (smaller K) than those beneath un-incised valley heads (Figure 2c). In addition, both numerical simulations and field measurements have shown that the layer of permeable fractured bedrock becomes thinner (smaller a) as topographic curvature increases (Flinchum et al., 2018; Moon et al., 2017). These effects are difficult to quantify and are sensitive to specific valley topography (Moon et al., 2017), preexisting fractures (Min et al., 2004), and ambient tectonic stresses (Clair et al., 2015), but sharper curvature is generally expected to reduce both the area and conductivity of the permeable zone (smaller T). This suggests that gradients in topographic curvature could cause gradients in transmissivity.

4. Predicting Stream Extension From Topography

We evaluated the relationship between the Laplacian topographic curvature (C) and drainage area ($C = \delta \ln A + C_0$) for each of the study sites (Figure 2i), and found that curvature coefficients (δ) are proportional to transmissivity scaling exponents (γ; Figure 3a; Table 1 and Text S1). At Caspar and Sagehen Creeks, which have consistent topographic curvature along the length of the ephemeral channel network, values of transmissivity exhibit only weak downstream trends. Meanwhile, at sites like McDonald Catchment 1 and Dunce Creek, strong gradients in valley transmissivity are accompanied by strong gradients in topographic curvature. While the linear relationship between δ and γ (Figure 3a) does not directly validate the mechanisms we have proposed to relate transmissivity and topographic curvature (Figure 2c), it does provide an empirical basis for estimating the transmissivity scaling exponent γ based on the topographic curvature coefficient δ. This empirical relationship can be substituted into equation (4):

$$L \propto Q_o^{\frac{\alpha}{k_1\delta+k_2+\theta+1}} = Q_o^{\beta} \quad \leftrightarrow \quad \beta = \frac{\alpha}{k_1\delta + k_2 + \theta + 1} \tag{5}$$

where $k_1 = 1.6 \pm 0.2$ km and $k_2 = -0.51 \pm 0.53$ for these 17 sites (Figure 3a). As catchment discharge varies, equation (5) predicts changes in stream length using only terms that can be measured directly from DEMs, nearly matching measured values of β for many sites without requiring any information about subsurface hydrological properties (Figure 3b). Because DEMs are available globally and at increasing resolution, equation (5) can be applied to any catchment where river discharge can be measured or estimated. However, the measurements of stream network dynamics that are required to verify this model have only been made for mountainous catchments in humid or semiarid climates. More observations are needed before this model (potentially with future modifications) can confidently be applied to other landscapes, including low-relief catchments or those in arid environments.

While these topographic metrics are likely to be useful for predicting stream network dynamics under wetting and drying (Figure 3b), the position and mobility of individual stream heads will often be controlled by bedrock and soil heterogeneities in each headwater valley (Godsey & Kirchner, 2014; Vaux, 1968; Whiting & Godsey, 2016). For example, stream heads are sometimes pinned in place by localized flow that brings water to the surface at permanent springs, and the positions of these fracture zones can be controlled by lithologic contacts or faults, rather than topography (Whiting & Godsey, 2016). However, most headwater valleys in mountainous terrain overlie pervasively fractured rock (Clarke & Burbank, 2010; Miller & Dunne, 1996), and topographic curvature should help set the aperture of these existing fractures (Min et al., 2004; Rutqvist, 2014; Figure 2c), thereby influencing which fractures host stream heads under different discharges. In other words, the spatial pattern of transport capacity that arises from intrinsic heterogeneities in soil and fractured bedrock will be noisy, but topography is expected to exert a persistent and predictable control on transport capacity that can be observed through the noise when averaging across many stream heads.

5. Feedback Between Erosion and Stream-Flow Emergence

We have so far focused on the physical mechanisms by which spatial patterns of slope, flow convergence, and topographic curvature can affect stream network extension and retraction over storm or seasonal time scales. Over time scales of valley incision (10^4 to 10^5 years), the reverse mechanistic relationships also exist: the extent of flowing stream networks determines the pattern of stream incision, thereby shaping patterns of slope, flow convergence, and topographic curvature. Based on the mechanisms proposed here (e.g., Figure 2), all of the topographic changes associated with localized stream incision—reduced slope (Howard et al., 1994), increased curvature (Roering et al., 2007), and increased flow convergence (Perron et al., 2012)—are expected to promote the emergence of streamflow. This suggests the possibility of a feedback mechanism that operates over geomorphic time scales, where streamflow incises bedrock valleys, reducing subsurface transport capacity and thus promoting surface flow and further valley incision. This positive feedback should tend to fix the stream network in place as fluvial landscapes evolve, leading to progressively more stable stream networks (smaller β). This could explain why our study catchments that retain evidence of Late Pleistocene glaciation have more dynamic drainage networks (larger β) than those where any prior glacial topography has been erased by fluvial incision (Gillespie & Clark, 2011; Whiting & Godsey, 2016; Figure 3b).

These findings suggest that topography and long-term patterns of erosion determine much of the dynamic response of flowing stream networks to catchment wetting and drying. The predictions of stream network extension and retraction presented here are only semimechanistic, because further work is needed to mechanistically relate topographic curvature to valley transmissivity. Nevertheless, based on empirical evidence from these 17 study sites, equation (5) appears to reliably predict, based on topographic data alone, how much stream networks will dynamically extend and retract in response to wetting and drying of the surrounding landscape. These predictions may, in turn, be combined with flow frequency curves in order to better constrain patterns of erosion, temporal variability in water-atmosphere gas exchange, and the mobility of freshwater organisms. Based on the availability of stream network measurements, this analysis was limited to landscapes that are relatively steep and humid, and our findings would most appropriately be applied to similar landscapes. However, the framework presented here may serve as a useful basis for extending these predictions to different landscapes as more field observations are collected.

Acknowledgments

This project was supported by Uniscientia Stiftung and by the ETH Zürich Foundation through an ETH Postdoctoral Fellowship to J.P.P. Stream network data (stream lengths and discharge, or β values) are available in the referenced studies. The topographic data used in this study are freely available through the USGS National Map Viewer. Detailed methods (Text S1) and Figures S1–S17 can be found in the supporting information. This manuscript benefited from the thoughtful comments of two anonymous reviewers.

References

Allen, G. H., & Pavelsky, T. M. (2018). Global extent of rivers and streams. *Science*, *361*, 585–588. https://doi.org/10.1126/science.aat0636

Allen, G. H., Pavelsky, T. M., Barefoot, E. A., Lamb, M. P., Butman, D., Tashie, A., & Gleason, C. J. (2018). Similarity of stream width distributions across headwater systems. *Nature Communications*, *9*, 610. https://doi.org/10.1038/s41467-018-02991-w

Aufdenkampe, A. K., Mayorga, E., Raymond, P. A., Melack, J. M., Doney, S. C., Alin, S. R., et al. (2011). Riverine coupling of biogeochemical cycles between land, oceans, and atmosphere. *Frontiers in Ecology and the Environment*, *9*, 53–60. https://doi.org/10.1890/100014

Blyth, K., & Rodda, J. C. (1973). A stream length study. *Water Resources Research*, *9*(5), 1454–1461. https://doi.org/10.1029/WR009i005p01454

Clair, J. S., Moon, S., Holbrook, W. S., Perron, J. T., Riebe, C. S., Martel, S. J., et al. (2015). Geophysical imaging reveals topographic stress control of bedrock weathering. *Science*, *350*, 534–538. https://doi.org/10.1126/science.aab2210

Clarke, A., Mac Nally, R., Bond, N., & Lake, P. S. (2008). Macroinvertebrate diversity in headwater streams: A review. *Freshwater Biology*, *53*, 1707–1721. https://doi.org/10.1111/j.1365-2427.2008.02041.x

Clarke, B. A., & Burbank, D. W. (2010). Bedrock fracturing, threshold hillslopes, and limits to the magnitude of bedrock landslides. *Earth and Planetary Science Letters*, *297*, 577–586. https://doi.org/10.1016/j.epsl.2010.07.011

Clubb, F. J., Mudd, S. M., Attal, M., Milodowski, D. T., & Grieve, S. W. D. (2016). The relationship between drainage density, erosion rate, and hilltop curvature: Implications for sediment transport processes. *121*, 1724–1745. https://doi.org/10.1002/2015JF003747

Costigan, K. H., Jaeger, K. L., Goss, C. W., Fritz, K. M., & Goebel, P. C. (2016). Understanding controls on flow permanence in intermittent rivers to aid ecological research: Integrating meteorology, geology and land cover. *Ecohydrology*, *9*, 1141–1153. https://doi.org/10.1002/eco.1712

Day, D. G. (1978). Drainage density changes during rainfall. *Earth Surface Processes*, *3*(3), 319–326. https://doi.org/10.1002/esp.3290030310

Dunne, T., & Black, R. D. (1970). An experimental investigation of runoff production in permeable soils. *Water Resources Research*, *6*(2), 478–490. https://doi.org/10.1029/WR006i002p00478

Flinchum, B. A., Steven Holbrook, W., Rempe, D., Moon, S., Riebe, C. S., Carr, B. J., et al. (2018). Critical zone structure under a granite ridge inferred from drilling and three-dimensional seismic refraction data. *Journal of Geophysical Research: Earth Surface*, *123*, 1317–1343. https://doi.org/10.1029/2017JF004280

Gillespie, A. R., & Clark, D. H. (2011). Glaciations of the Sierra Nevada, California, USA. *Developments in Quaternary Sciences*, *15*, 447–462. https://doi.org/10.1016/B978-0-444-53447-7.00034-9

Godsey, S. E., & Kirchner, J. W. (2014). Dynamic, discontinuous stream networks: Hydrologically driven variations in active drainage density, flowing channels and stream order. *Hydrological Processes*, *28*, 5791–5803. https://doi.org/10.1002/hyp.10310

Goulsbra, C., Evans, M., & Lindsay, J. (2014). Temporary streams in a peatland catchment: Pattern, timing, and controls on stream network expansion and contraction. *Earth Surface Processes*, *39*, 790–803. https://doi.org/10.1002/esp.3533

Gregory, K. J., & Walling, D. E. (1968). The variation of drainage density within a catchment. *Hydrological Sciences Journal*, *13*(2), 61–68. https://doi.org/10.1080/02626666809493583

Howard, A. D., Dietrich, W. E., & Seidl, M. A. (1994). Modeling fluvial erosion on regional to continental scales. *Journal of Geophysical Research*, *99*(B7), 13,971–13,986. https://doi.org/10.1029/94JB00744

Jensen, C. K., McGuire, K. J., & Prince, P. S. (2017). Headwater stream length dynamics across four physiographic provinces of the Appalachian highlands. *Hydrological Processes*, *31*, 3350–3363. https://doi.org/10.1002/hyp.11259

Jensen, C. K., McGuire, K. J., Shao, Y., & Andrew Dolloff, C. (2018). Modeling wet headwater stream networks across multiple-flow conditions in the Appalachian highlands. *Earth Surface Processes*, *43*, 2762–2778. https://doi.org/10.1002/esp.4431

Kennedy, V. C., Jackman, A. P., Zand, S. M., Zellweger, G. W., & Avanzino, R. J. (1984). Transport and concentration controls for chloride, strontium, potassium and lead in Uvas Creek, a small cobble-bed stream in Santa Clara County, California, USA: 1. Conceptual model. *Journal of Hydrology*, *75*(1–4), 67–110. https://doi.org/10.1016/0022-1694(84)90046-5

Kirby, E., & Whipple, K. X. (2012). Expression of active tectonics in erosional landscapes. *Journal of Structural Geology*, *44*, 54–75. https://doi.org/10.1016/j.jsg.2012.07.009

Lovill, S. M., Hahm, W. J., & Dietrich, W. E. (2018). Drainage from the critical zone: Lithologic controls on the persistence and spatial extent of wetted channels during the summer dry season. *Water Resources Research*, *54*, 5702–5726. https://doi.org/10.1029/2017WR021903

Miller, D. J., & Dunne, T. (1996). Topographic perturbations of regional stresses and consequent bedrock fracturing. *Journal of Geophysical Research*, *101*(B11), 25,523–25,536. https://doi.org/10.1029/96JB02531

Min, K.-B., Rutqvist, J., Tsang, C.-F., & Jing, L. (2004). Stress-dependent permeability of fractured rock masses: A numerical study. *International Journal of Rock Mechanics and Mining*, *41*, 1191–1210. https://doi.org/10.1016/j.ijrmms.2004.05.005

Moglen, G. E., Eltahir, E. A. B., & Bras, R. L. (1998). On the sensitivity of drainage density to climate change. *Water Resources Research*, *34*(4), 855–862. https://doi.org/10.1029/97WR02709

Moon, S., Perron, J. T., Martel, S. J., Holbrook, W. S., & St Clair, J. (2017). A model of three-dimensional topographic stresses with implications for bedrock fractures, surface processes, and landscape evolution. *Journal of Geophysical Research: Earth Surface*, *122*, 823–846. https://doi.org/10.1002/2016JF004155

Perron, J. T., Richardson, P. W., Ferrier, K. L., & Lapôtre, M. (2012). The root of branching river networks. *Nature*, *492*, 100–103. https://doi.org/10.1038/nature11672

Roberts, M. C., & Archibold, O. W. (1978). Variation of drainage density in a small British Columbia watershed. *Journal of the American Water Resources Association*, *14*(2), 470–476. https://doi.org/10.1111/j.1752-1688.1978.tb02183.x

Roberts, M. C., & Klingeman, P. C. (1972). The relationship of drainage net fluctuation and discharge. In *22nd International Geographical Congress* (Vol. 1, pp. 189–191). Montréal: Les Presses de l'Université de Montréa.

Roering, J. J., Perron, J. T., & Kirchner, J. W. (2007). Functional relationships between denudation and hillslope form and relief. *Earth and Planetary Science Letters*, *264*, 245–258. https://doi.org/10.1016/j.epsl.2007.09.035

Rutqvist, J. (2014). Fractured rock stress-permeability relationships from in situ data and effects of temperature and chemical-mechanical couplings. *Geofluids*, *15*, 48–66. https://doi.org/10.1111/gfl.12089

Shaw, S. B. (2016). Investigating the linkage between streamflow recession rates and channel network contraction in a mesoscale catchment in New York state. *Hydrological Processes*, *30*, 479–492. https://doi.org/10.1002/hyp.10626

Tucker, G. E., & Bras, R. L. (1998). Hillslope processes, drainage density, and landscape morphology. *Water Resources Research*, *34*, 2751–2764. https://doi.org/10.1029/98WR01474

Vaux, W. G. (1968). Intragravel flow and interchange of water in a streambed. *The United States Fish and Wildlife Service Fish B*, *66*(3), 479–489.

Ward, A. S., Schmadel, N. M., & Wondzell, S. M. (2018). Simulation of dynamic expansion, contraction, and connectivity in a mountain stream network. *Advances in Water Resources*, *114*, 64–82. https://doi.org/10.1016/j.advwatres.2018.01.018

Whiting, J. A., & Godsey, S. E. (2016). Discontinuous headwater stream networks with stable flowheads, Salmon River basin, Idaho. *Hydrological Processes*, *30*, 2305–2316. https://doi.org/10.1002/hyp.10790

Wigington, P. J., Moser, T. J., & Lindeman, D. R. (2005). Stream network expansion: A riparian water quality factor. *Hydrological Processes*, *19*, 1715–1721. https://doi.org/10.1002/hyp.5866

Wondzell, S. M. (2011). The role of the hyporheic zone across stream networks. *Hydrological Processes*, *25*, 3525–3532. https://doi.org/10.1002/hyp.8119

Zimmer, M. A., & McGlynn, B. L. (2017). Ephemeral and intermittent runoff generation processes in a low relief, highly weathered catchment. *Water Resources Research*, *53*, 7055–7077. https://doi.org/10.1002/2016WR019742

Zimmer, M. A., & McGlynn, B. L. (2018). Lateral, Vertical, and Longitudinal Source Area Connectivity Drive Runoff and Carbon Export Across Watershed Scales. *Water Resources Research*, *54*, 1576–1598. https://doi.org/10.1002/2017WR021718